Internal Dielectric Transduction of a 4.5 GHz Silicon Bar Resonator

Dana Weinstein and Sunil A. Bhave

OxideMEMS Lab, Cornell University, Ithaca, NY, U.S.A.

Abstract

This paper presents experimental verification of frequency scaling in an internal dielectric transduced resonator. A silicon bar resonator is excited in its 3rd and 9th longitudinal harmonic modes at 1.53 and 4.51 GHz, respectively. The resonator demonstrates a 2 dB improvement in transduction efficiency in its 9th harmonic relative to its 3rd harmonic, normalized to the quality Q of the resonance. This result is in close agreement with theory, promising low-impedance transduction of silicon bulk acoustic resonators at frequencies exceeding 10 GHz.

Introduction

Semiconductor electromechanical resonators, with quality factors (Q) often exceeding 10,000, provide a low-power, small footprint, CMOS-compatible alternative to various electrical components in wireless communication and signal processing. Much effort has been spent in the micromechanical resonator community to design devices in the 1 MHz-1GHz frequency range, focusing on sensors, frequency synthesizers, and radio front-end applications. This work focuses on scaling electrostatic acoustic resonators to the SHF and EHF bands of the radio spectrum. Resonator applications in this frequency range include microwave oscillators, with particular emphasis on low-power local clock distribution in microprocessors.

In this paper, we present the highest acoustic frequency measured in silicon resonators to date at 4.51 GHz. We propose and experimentally verify the optimal design for 'internal dielectric transduction' of longitudinal bulk mode MEMS resonators. This transduction mechanism increases in efficiency as the dielectric thickness approaches the acoustic half-wave length in silicon. With dielectric films at positions of maximum strain (minimum displacement) in the resonator, a 4.51 GHz resonator is demonstrated with a 9.8 dB signal enhancement relative to its performance at 1.53 GHz. Our analysis and experimental verification of improved resonator performance at higher frequency promise scaling of MEMS resonators to previously unattainable frequencies.

The difference between 'internal' [1] and 'external' [2] dielectric transduction determines their capabilities at higher frequencies. Both mechanisms employ dielectric drive and sense transducers. External transduction assumes free boundary conditions (zero stress) at the dielectric interface, driving at a frequency corresponding to a resonant mode with maximum displacement at the dielectric, and necessitating maximum acoustic mismatch between the dielectric and resonator bulk. This boundary condition at the dielectric interface results in an observed transduction loss, particularly
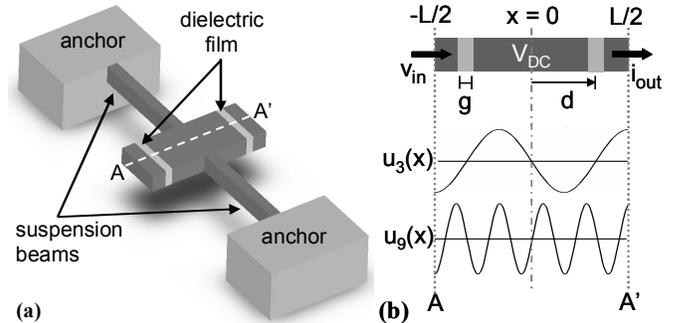

Fig. 1. (a) Schematic of dielectrically transduced free-free longitudinal bulk mode resonator. (b) Cross section of bar resonator along A-A'. A bias voltage V_{DC} is applied to the resonator. An AC voltage v_{in} on one end drives resonance, while an output current i_{out} is measured at the other end. The normalized amplitudes of the 3rd and 9th longitudinal mode harmonics are displayed.

at higher frequencies, the exact cause of which is yet to be explained.

On the other hand, internal transduction incorporates the dielectric film into the resonant mode shape. This generally involves the assumption of a close acoustic match between the bulk resonator and dielectric film. In practice, a mismatch in acoustic impedance between the dielectric and resonator material results in a shift of the resonant frequency, and can easily be compensated by altering the dimensions of the resonator.

Optimization of Dielectric Transduction

A longitudinal-mode bar resonator is driven and sensed electrostatically with thin vertical dielectric layers, as shown in Figure 1. The resonator body is biased to V_{DC}, and a harmonic excitation of amplitude v_{in} is applied to the drive electrode at resonant frequency. The longitudinal resonant displacement induced in the resonator follows

$$u(x,t) = U_0 e^{i2\pi \cdot f_n t} \sin(k_n x), \quad \text{n odd,} \tag{1}$$

where $k_n = n\pi/L$ is the resonance wave number and $f_n = (n/2L)\sqrt{Y/\rho}$ is the resonant frequency. Y and ρ are the Young's modulus and mass density of the resonator, respectively. The 2-port motional impedance $R_X \equiv v_{in}/i_{out}$ for the nth harmonic is given by [1]

$$R_X = \frac{n\pi\sqrt{Y\rho}}{2QA\varepsilon_f^2 V_{DC}^2} \frac{g^4}{\cos^2(k_n d)\sin^2(k_n g/2)}. \tag{2}$$
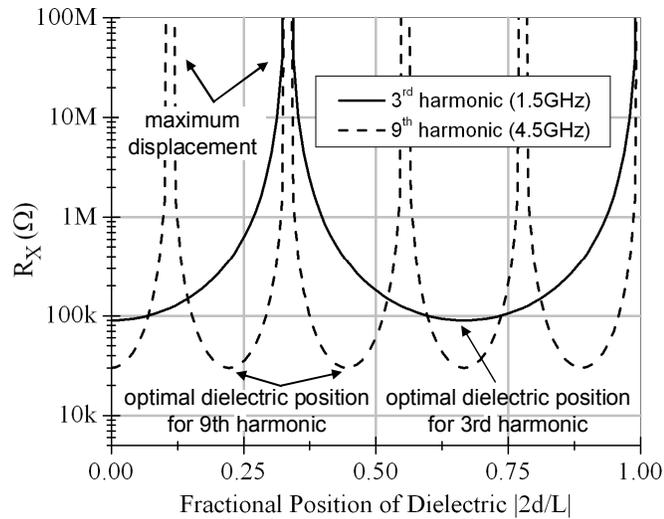
Here, ε_f is the dielectric permittivity, g is the dielectric thickness, d is the position of the dielectric along the bar, and A is the transduction area. Equation 2 provides guidelines for optimizing the bulk-mode resonator using internal dielectric transduction. As expected, the quartic dependence of the

motional impedance on dielectric thickness necessitates the thinnest dielectric possible. This is defined by limitations in fabrication and material properties. The formulation for R_X indicates that the position of both drive and sense dielectric films should be centered at a displacement minimum, or strain maximum. This choice for the position of the dielectric films sets $\cos^2(k_n d) = 1$, minimizing R_X with respect to d.

The $\sin^2$ term in the denominator of Equation 2 results from the modal displacement of the dielectric-bulk resonator interface. Kaajakari et al [3] have noted that this factor degrades transduction efficiency considerably at low frequencies, where the acoustic wavelength $\lambda \gg g$. However, as the resonator scales to higher frequencies, and $\lambda/2 \to g$, the $\sin^2$ term in the denominator approaches unity, reducing motional impedance. Consequently, for a fixed dielectric thickness g determined by fabrication limitations, there is an optimal frequency of operation with acoustic wavelength $\lambda = 2 \cdot g$. This frequency scaling result converges to an FBAR-like resonator or the Bragg reflector for a solid-mounted bulk acoustic wave (BAW) resonator, stacking multiple dielectrics of thickness $\lambda/2$ between conductive layers of the same thickness.

Figure 2 presents the analytical R_X of the 3rd and 9th harmonics of an internally transduced longitudinal bar, varying the dielectric position along the length of the resonator. As shown in the plot, minima in the motional impedance occur for points of maximum strain (minimum displacement). The large spatial range near the displacement minima over which R_X is low allows for fabrication of reliable devices despite misalignment tolerances.

The quartic dependence of R_X on the dielectric thickness g indicates that to minimize R_X, the thinnest possible

dielectric film should be used. The increased frequency of vibration in higher harmonics (and thus the increased wave number k_n) means that as the acoustic half-wavelength approaches g, the $\sin^2$ term in the denominator of Equation 2 approaches unity, reducing R_X. This effect outweighs the linear dependence of the motional impedance on the order of the harmonic, resulting in an overall reduction in R_X for higher harmonics.

The position of the dielectric can be exploited to design resonators which preferentially excite higher harmonics. For example, if the dielectric film is placed at a displacement node of the 9th harmonic near the center of the resonator, then the motional impedance of lower harmonics will be too high to excite vibrations, and spurious modes will be minimized. In this study, the dielectric is placed at the coincidence of displacement nodes for both 3rd and 9th harmonics, optimizing transduction for both modes.

Fabrication and Measurement Technique

The resonators were fabricated in a combined SOI-polysilicon process using a 15 nm silicon nitride film for transduction, as detailed in Figure 3. (1) The device layer of an SOI wafer is first patterned in DRIE with a hard oxide mask. The device layer is 2.5 μm thick. (2) A 15 nm conformal LPCVD silicon nitride film is then deposited to form the transduction dielectric. (3) A layer of n+ polysilicon >3 μm thick is deposited, annealed, and (4) smoothed with CMP. (5) A second hard oxide mask is then deposited and patterned to (6) etch the polysilicon and define the final resonator shape. (7) The resonators are released in an HF timed etch followed by a critical-point dry (CPD) step to prevent stiction. Though the outer rim of silicon nitride is removed in the HF release step (Fig. 4 inset), the nitride remains in the majority of the transduction area as evidenced by capacitive measurements.

Suspension beams for the resonators are designed at quarter-wave length to minimize anchor losses for both 3rd and 9th harmonics and dampen spurious modes. The mode shape and SEM of the resonator are presented in Figure 4. As seen in the figure, the non-ideal routing beams of the input and output electrodes of the resonator distort the one-dimensional longitudinal mode shape assumed for transduction calculations and frequency scaling. The distorted mode, which couples an 8th harmonic surface mode to the original longitudinal resonance, slightly degrades the transduction efficiency due to a small cancellation in signal from the summed contribution of both tensile and compressive strain in the dielectric film. However, the primary contribution to the capacitive sensing results from the longitudinal component of the dielectric strain, yielding transduction close to that described by the theory in [1].

Capacitive electromechanical resonators can be used as passive mixers due to their nonlinear electrostatic actuation. The resonator can thus be characterized by measuring the conversion loss of the mixer. A scalar mixing measurement
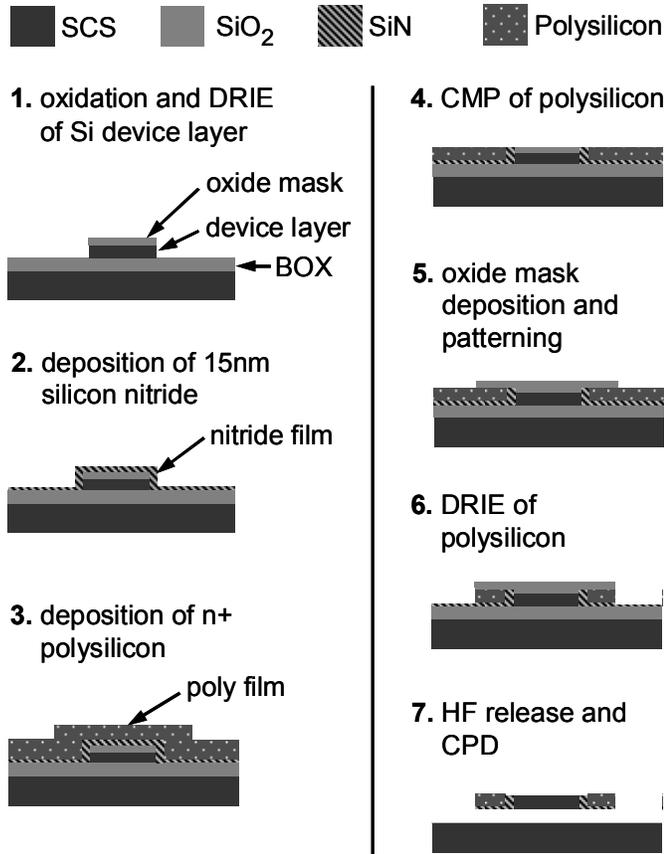

Fig. 2. Analytical results of R_X as a function of fractional dielectric position $|d/(L/2)|$ for the 3rd and 9th longitudinal harmonic modes of a 8.5μm long × 40μm wide × 2.5 μm tall bar. Nitride thickness is 15 nm, $V_{DC} = 5$ V, and $\varepsilon_f = 7\,\varepsilon_0$. A Q of 5000 is assumed. The R_X minima occur at displacement nodes of the resonant mode. Enhanced transduction at higher frequency yields a 3× improvement in R_X from the 3rd to the 9th harmonic modes.

1. oxidation and DRIE of Si device layer

oxide mask
device layer
← BOX

2. deposition of 15nm silicon nitride

nitride film

3. deposition of n+ polysilicon

poly film

4. CMP of polysilicon

5. oxide mask deposition and patterning

6. DRIE of polysilicon

7. HF release and CPD

Fig. 3. Micro-fabrication process for internal dielectric transduced resonators.

Fig. 4. *Left:* Modal analysis of 3rd harmonic resonant mode shape of the bar resonator, simulated in Ansys. The non-ideal routing beams distort the longitudinal mode shape. Nonetheless, the longitudinal deformation along the dielectric film is preserved. *Right:* Scanning Electron Micrograph of a dielectrically transduced silicon bar resonator (8.5μm long × 40μm wide × 2.5 μm tall). The inset image shows the thin gap between the polysilicon and single crystal regions of the resonator. Though the outer rim of silicon nitride is removed in the HF release step, the nitride remains in the majority of the transduction area as evidenced by capacitive measurements.

Fig. 5. Schematic of scalar mixer measurement of the 3-port MEMS resonator. The resonator (DUT) acts as a mixer for the input RF and LO signals. The resonance is detected at RF − LO, thus preventing effects of feed-through capacitance in the transmitted frequency response.

(Figure 5) similar to [4] using an Agilent PNA was performed to obtain the frequency response of the resonator. A scalar mixer calibration technique traditionally used to characterize RF mixers was implemented to measure the performance of the high frequency resonators. This method circumvents capacitive losses and parasitic transmission-line resonances in the probe-pads and routing of the 3-port MEMS device and provides an accurate measurement of mechanical Q at frequencies well above 1 GHz [5].

Standard 2-port measurements for which the input and measured frequencies are the same require de-embedding structures (namely, short, open, and through structures) to cancel parasitic capacitance, inductance, and resistance from the device measurement. In 3-port scalar mixing measurements, however, parasitic feedthrough currents occur off the resonant (measured) frequency. Since no de-embedding is performed in this measurement, there exists a parasitic resistance from the probe tips to and from the device. The resistance decreases the total signal strength, resulting in an uncalibrated absolute performance of the device. The absolute R_X of the resonator cannot be extracted from the measurement without resistive de-embedding, and will appear higher than expected. However, for the purposes of this experiment, the absolute performance of the device is not critical. Rather, the relative performance of the resonator
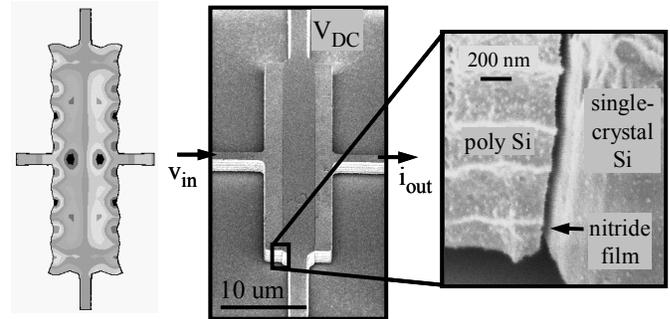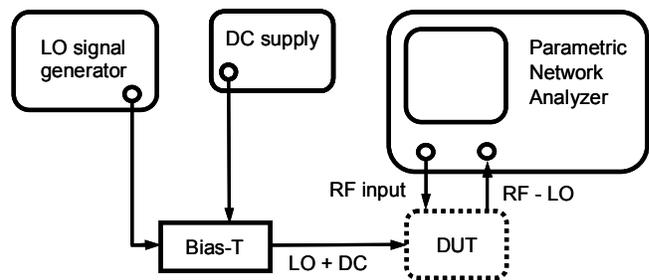
operating at two different frequencies is investigated. Since the same device is probed for both harmonics and the probe tips remain fixed for the entire measurement, the resistive path from the probe tip to the device remains constant. A comparison of resonance at both harmonics therefore provides useful information about the relative transduction efficiency of the two resonant modes.

Experimental Results

Devices were tested at room temperature in a Lakeshore vacuum probe station, applying a 5V bias, -10 dBm LO, and 0 dBm RF input. The resonator's frequency response is presented in Figure 6. The LO leakage of the device (grey traces) was obtained by setting the bias voltage to 0V. Acoustic resonance was excited when a 5V bias was applied (black traces). The 9th harmonic, with a Q of 11,200, shows a 9.8 dB signal improvement over the 3rd harmonic, with a Q of only 1,700. The 4.51 GHz resonance has an $f \cdot Q$ product of 5.1×10^{13}.

The motional impedance in Equation 2 is inversely proportional to Q. To extract the relationship of transducer efficiency with frequency scaling, we normalize the scalar conversion loss at resonance by the Q of the harmonic. With this normalization, we can directly compare the performance

417
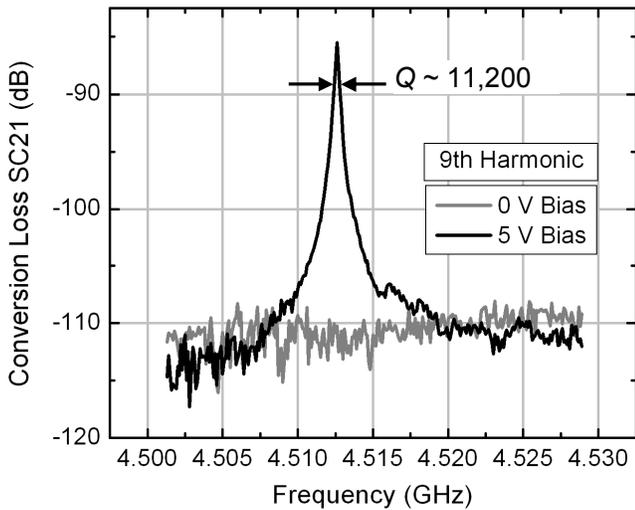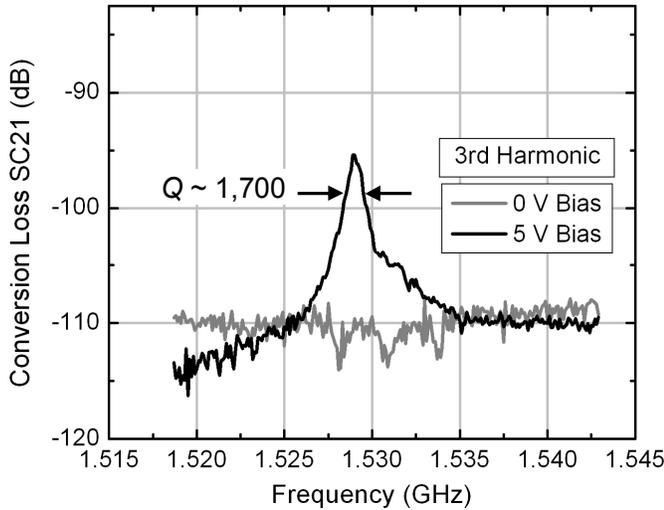
Fig. 6. Measured frequency response of 3rd and 9th harmonic resonance of the silicon bar resonator. The grey traces (0 V) indicate the LO leakage of the device. Applying a 5 V bias excites acoustic resonance, shown in black. The 9th harmonic exhibits a 9.8 dB absolute improvement in signal strength over the 3rd harmonic mode, with a Q increase of 6.6×. Normalizing the resonant peaks by Q, we extract a 2 dB enhancement of transduction efficiency in the 4.5 GHz resonance relative to the 1.5 GHz resonant mode.

of the two harmonics. Taking this into account, the 4.51 GHz normalized signal improves by 2 dB relative to the 1.53 GHz normalized response. The analytical model predicts a ~3× improvement in motional impedance between the 3rd and 9th harmonics, translating to a 4.7 dB signal improvement. The discrepancy may be due to small misalignment (< 200 nm) and the width-distortion of the longitudinal mode-shape (Figure 4). In particular, the transducer efficiency is more sensitive to misalignment of the dielectric film position at higher harmonics, since the misalignment corresponds to a larger fraction of the total wavelength at higher frequencies. Therefore, a misalignment in the device under test degrades the performance of the 9th harmonic more than the 3rd harmonic, contributing to a smaller relative transduction enhancement than expected.

Conclusion

A 4.51 GHz longitudinal bar resonator is demonstrated, marking the highest frequency measured to date in silicon. The 3rd and 9th harmonics of longitudinal vibration were excited in a silicon bar resonator, demonstrating a 9.8 dB absolute improvement in signal strength and 2 dB (Q-normalized) enhancement in transduction efficiency for the 9th harmonic (4.51 GHz) relative to the 3rd harmonic (1.53 GHz). The 4.51 GHz resonance exhibits an $f \cdot Q$ product of 5.1×10^{13}. These results indicate improved resonator performance with increased frequency, providing a means of scaling MEMS resonators to previously unattainable frequencies in silicon.

References:

[1] D. Weinstein and S.A. Bhave, "Internal dielectric transduction: optimal position and frequency scaling," IEEE Transactions on Ultrasonics, Ferroelectrics, and Frequency Control (in press).

[2] Y.-W. Lin, S.-S. Li, Y. Xie, Z. Ren, C.T.-C. Nguyen, "Vibrating Micromechanical Resonators with Solid Dielectric Capacitive Transducer Gaps," IEEE International Frequency Control Symposium 2005, pp.128-134.

[3] V. Kaajakari, A.T. Alastalo, T. Mattila, "Electrostatic Transducers for Micromechanical Resonators: Free Space and Solid Dielectric", IEEE Transactions on UFFC **53** (12), pp. 2484-89 (2006).

[4] A.-C. Wong, H. Ding, C.T.-C. Nguyen, "Micromechanical Mixer+ Filters," IEEE International Electron Device Meeting 1998, pp. 471-474.

[5] Agilent Technologies - Frequency Converter Application *http://na.tm.agilent.com/pna/help/PNAWebHelp/FreqOffset/FCA.htm* cited: September 10, 2007.